Developing an optimum computer-designed multispectral system comprising a monochrome CCD camera and a liquid-crystal tunable filter

Miguel A. López-Álvarez,[1,*] Javier Hernández-Andrés,[2] and Javier Romero[2]

[1]Hewlett-Packard Spain, Large Format Printing Division, 08174 Sant Cugat del Vallès, Barcelona, Spain

[2]Colour Imaging Laboratory, Departamento de Óptica, Universidad de Granada, 18071 Granada, Spain

*Corresponding author: migangel@ugr.es

In a previous work [J. Opt. Soc. Am. A **24**, 942 (2007)] we made a complete theoretical and computational study of the influence of several parameters on the behavior of a planned multispectral system for imaging skylight, including the number of sensors and the spectral estimation algorithm. Here we follow up this study by using all the information obtained in the computational simulations to implement a real multispectral imaging system based on a monochrome CCD camera and a liquid-crystal tunable filter (LCTF). We were able to construct the optimum Gaussian sensors found in the simulations by adjusting the exposure times of some of the transmittance modes of the LCTF, hence obtaining really accurate spectral estimations of skylight with only a few optimum sensors. © 2008 Optical Society of America

OCIS codes: 150.2950, 280.0280, 040.0040.

1. Introduction

Over the past ten years several authors have contributed to the development of the theory behind multispectral imaging systems [1–6], and in doing so have proved the reliability of these devices for making accurate estimations of spectral-power distributions (SPDs) in every pixel of the imaged scene [1]. Most of these works focus on recovering the spectral reflectance of objects or the combined color signal [7–9], but little information has been published about spectral estimation of natural illuminants [10–12]. The advantages of using such systems instead of traditional spectroradiometers are numerous. For example, we can obtain a radiance spectrum for each pixel of the imaging matrix, typically a charge-coupled device (CCD) or a complementary-metal-oxide-semiconductor device (CMOS) [13]. Moreover, multispectral systems are cheaper, lighter, and more portable than classical spectroradiometers.

Here we focus our interest on studying skylight, an important natural illuminant [14,15], from the spectral curves of which we can extract information about climate parameters such as the optical depth or the Angstrom exponent [15], which inform us about the size and concentration of aerosol particles. Recently we also suggested the possibility of developing computer algorithms for automatic cloud detection and classification based on the spectral information estimated from multispectral images of the sky. A huge database of multispectral skylight images could be interesting for scientists of many disciplines, since it would provide images of the entire skydome with high spatial and spectral resolution that could be used in many areas of research.

In previous works [10,11] we published a complete theoretical study about a planned optimum multispectral system for the spectral imaging of skylight. By developing computational simulations we

obtained very interesting results concerning the influence on the behavior of the multispectral system of several parameters, such as the spectral responsivity of its sensors, the number and type of sensors, the spectral estimation method and linear bases chosen, the number and quality of training spectra, and the noise that always affects any electronic device. As a result we found that when certain values for these parameters were set we could make very accurate spectral reconstructions. Thus, we now intend to use these previous results to build a prototype of this optimum multispectral system by using a cooled, 12 bit, monochrome CCD camera (Model Retiga QI-maging SRV1340) and an LCTF (Model Varispec, from CRi). Given the possibility of making a complete calibration [16] of the elements of the multispectral system, we also obtained spectral measurements of skylight radiance by direct radiometric wavelength sampling. We show how the optimum configuration found for the system in the computational study provides better spectral recoveries and results much faster.

In Section 2 we resume the results of previous papers [10,11] by showing the optimum configuration of the system that can be implemented when we use the devices available in our laboratory. We also describe the training and test sets of experimental measurements of spectral skylight used in this study. In Section 3 we show how to obtain spectral measurements with the CCD camera and the LCTF when these devices are correctly calibrated (the measurement process is done by developing a direct radiometric wavelength sampling, which is here described in detail), and we plot the results when using the system in this configuration. In Section 4 we obtain spectral estimations by using a regression model with the 33 channels or transmittance modes [1] of the LCTF and compare it with the results obtained when we use the optimum configuration for the system (Section 5). Finally, we give some ideas about future work and discuss the pros and cons of each of the configurations proposed for the multispectral system.

2. Computational Results

We used a model proposed by Maloney and Wandell [17], which is a widely accepted [1–9] theoretical model of the responses of the camera, ρ (a column vector of k rows corresponding to the k channels or sensors available), when a given radiance spectrum, E (a column vector of N rows corresponding to the N different wavelengths sampled in the visible spectrum), impinges on it. Thus,

$$\rho = R^t E + \sigma, \qquad (1)$$

where R is an $N \times k$ matrix containing the spectral responsivities of the k sensors at N sampled wavelengths (superscript t denotes its transpose), and σ is a k row vector of uncorrelated components of noise that affect each sensor separately [1,10].

The goal here is to recover spectrum E from responses ρ of the sensors. Different spectral estimation methods [3–5,10,17,18] have been used to try to solve this problem. Our previous study [10] was focused on comparing the accuracy of the spectral reconstructions obtained with each of these methods when the optimum sensors found for them in each case were used. We found that the Linear Pseudoinverse method (sometimes erroneously called the Wiener method because of their mathematical similarity) and the Imai–Berns method [3] provided good spectral reconstructions, with the additional advantage—compared to other spectral estimation methods—that it is not necessary to know the spectral responsivity of camera R in practical situations where computer simulations are not involved. These two methods were fast in their calculations and also very robust against noise. The only drawback of the Imai–Berns method is that it needs a representative linear basis of spectra for training, but this may be an advantage in situations with high noise, because a reduction of the dimensionality can be achieved by using basis vectors and this may help to reduce the influence of noise [5,9,10]. The task of calculating a basis is fairly easy by means of principal component analysis [1] (PCA), nonnegative matrix factorization (NMF) [19] or the independent component analysis (ICA) [20] of a training set of spectral measurements. These mathematical tools coincide in providing a set of vectors that can be used to express a given spectrum as a linear combination:

$$E = V\epsilon, \qquad (2)$$

where V is an $N \times n$ matrix containing the first n vectors used for reconstructing N wavelengths (n is always less than or equal to N and is usually chosen to equal k, the number of sensors, which often gives the best results [3,10]). Vector ϵ is an n rowed vector that contains the coefficients of the linear combination.

We use the Imai–Berns method here because with our LCTF we can build the optimum set of five sensors found with this method when the noise simulated at the camera gives a value of 26 dB for the signal-to-noise ratio (SNR). This noise level was really close to the real noise in our camera, which was estimated by measuring the variance when imaging an integrating sphere [16] that serves as a perfectly homogeneous and constant object. As some authors have indicated [5], the closest the estimated noise used to find the optimum sensors is to the real noise level, the better those filters will be when implemented with the real system. We must point out that using only the Imai–Berns method does not mean that we cannot use other spectral estimation methods with our system, just that the optimum sensors found for the other methods studied are not achievable with our LCTF.

In Fig. 1 we show the 33 transmittance modes measured for our LCTF in the laboratory. Figure 2 shows the five optimum sensors that we intend to implement and how these sensors can be obtained with seven
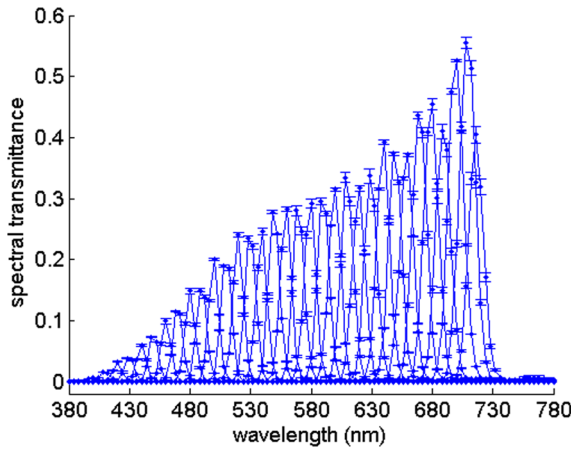
Fig. 1. (Color online) Spectral transmittance of the 33 modes of the Varispec liquid-crystal tunable filter measured three times in our laboratory (error bars show the standard deviation obtained at each sampled wavelength).

modes of our filter by adjusting the exposure times and summing up the contributions of modes 3, 4, and 5 (corresponding to the third optimum sensor), where the spectral responsivity of the CCD (shown in Fig. 3) has been taken into account. We also use the Imai–Berns method and the Linear Pseudoinverse method with the 33 channels (Section 4) already available with our multispectral system to compare the quality of the spectral reconstructions when we use only five optimum sensors (Section 5).

We need to train the system before using the two spectral estimation methods mentioned above, since these algorithms use the information obtained from a training set of spectra to provide good spectral reconstructions from the sensors' responses. For the Imai–Berns method we directly establish a relationship between the sensors' responses ρ and coefficients ϵ, which now includes a column in ρ_{ts} and ϵ_{ts} for each of the m training spectra (subscript ts stands for training spectra), and we obtain
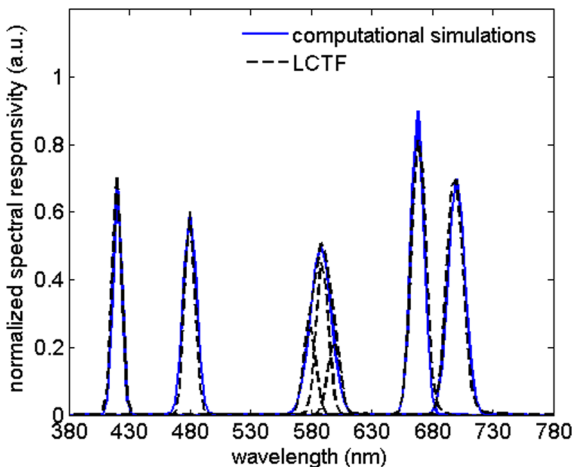

Fig. 2. (Color online) Five optimum sensors found in the computational simulations (solid line) for the Imai–Berns method with a SNR equal to 26 dB. Seven transmittance modes of the LCTF (dashed line) used to implement the theoretical optimum sensors.
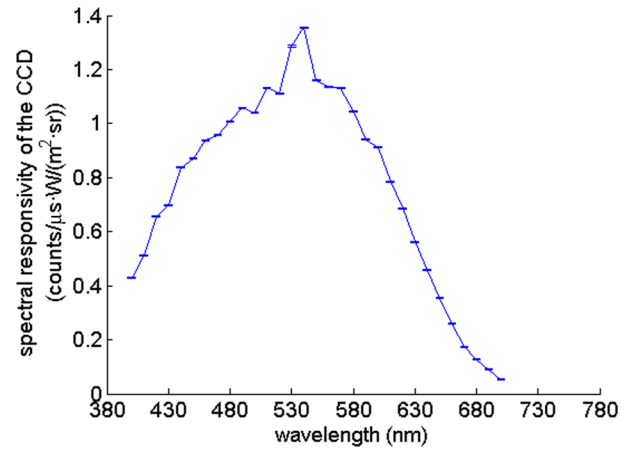

Fig. 3. (Color online) Spectral responsivity of the CCD camera (Model Retiga QImaging SRV1394) measured at our laboratory. Error bars show the uncertainty in these measurements.

$$\varepsilon_{ts} = G\rho_{ts}, \qquad (3)$$

where matrix G is an $n \times k$ matrix that is determined empirically by a least-squares analysis of the training-spectra measurements. Hence it is not necessary to measure spectral sensitivities R of the camera to use this method with real sensor-response measurements [10]. We can estimate G via a least-squares analysis by pseudoinverting the $k \times m$ matrix, ρ_{ts}:

$$G = \varepsilon_{ts}\rho_{ts}^{+}. \qquad (4)$$

In our case, the recovered skylight spectrum is simply calculated in this method from sensors' responses ρ by

$$E_R = VG\rho. \qquad (5)$$

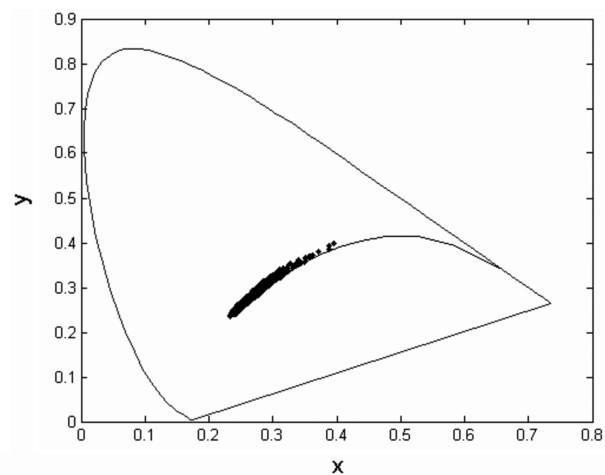Here the information provided by the training spectra is included in V and in G.

If we use the Linear Pseudoinverse method, we must establish a relationship directly between sensors' responses of the training set ρ_{ts} and training spectra E_{ts}:
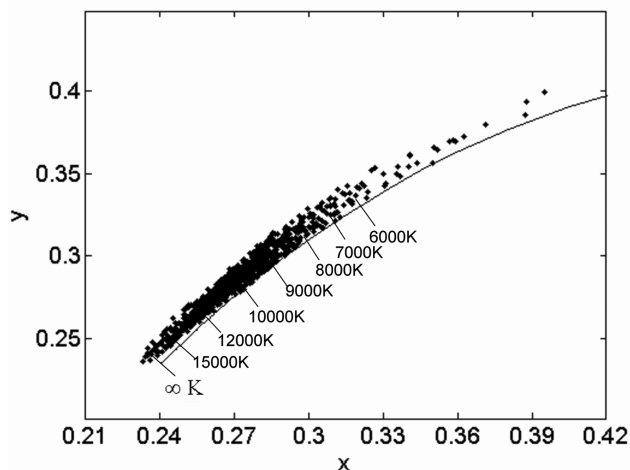
$$W = E_{ts}\rho_{ts}^{+}. \qquad (6)$$

Thus we can obtain spectral estimations with the Linear Pseudoinverse method exactly in the way shown in Eq. (5) by replacing VG with the matrix W.

It is desirable to use different sets of spectral measurements as training and test sets. As the training set in this study we use a database of 1567 spectral skylight measurements taken by our group between 1997 and 1999 [21] in Granada (Spain, 37.16° N, 3.60° W, 680 m.a.s.l.) with a LICOR spectrorradiometer, at many different solar elevations, with different relative azimuths towards the sun and during different seasons of the year; each spectrum ranged from 380 to 780 nm in 5 nm steps. By that time we had not yet constructed our multispectral system and so we have no experimental information on responses of the camera

ρ_{ts} but we can calculate the theoretical responses of our multispectral system (which is correctly calibrated) to these spectra and use them in Eq. (4) to obtain the matrix G. This step is explained in detail in Section 4. As a test set, we use a set of 125 spectral measurements also taken in Granada in 2007 over a period of 7 months, which now does include the information of the experimental camera responses, ρ. This set of spectra was measured simultaneously with our multispectral system and a SpectraScan PR650 spectroradiometer between 380 and 780 nm in 4 nm steps. We try to recover spectra E of the test set by using the information registered with camera ρ and the information provided by the training set (E_{ts}, ϵ_{ts}, and the calculated ρ_{ts}; these parameters are needed to calculate matrix G). In Fig. 4 we show the chromaticity coordinates, in the CIE-31 space, of the 1567 skylight spectra belonging to the training set (its correlated color temperatures (CCT) ranging from 3500 K to infinity; we must say that two measurements of this set do not have an associated CCT because their chromaticities lie too far from
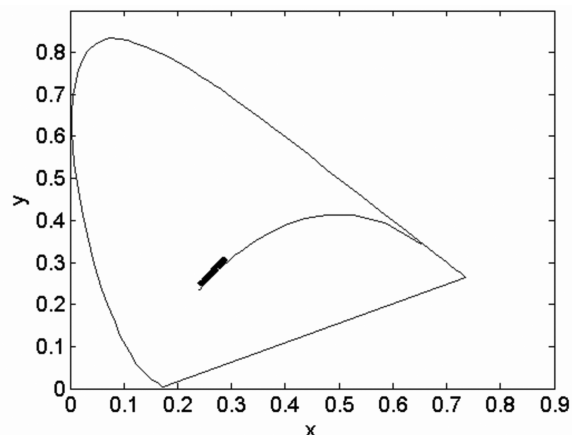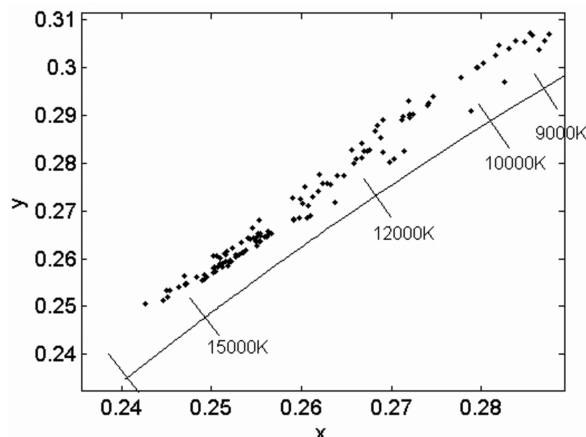
the Planckian locus [21]), while in Fig. 5 we show the same diagram for the test set of 125 measurements (with CCTs ranging from 8300 K to 32,000 K).

3. Spectral Measurements of Skylight by Direct Radiometric Sampling

In Figs. 1 and 3 we show the results of calibrating the LCTF and the CCD camera. Thus we have two precise devices that can be used together to obtain spectroradiometric measurements by taking advantage of two things: the radiometric information provided by the CCD camera and the narrow spectral band in the visible range selected with the LCTF. The main assumptions here are two. First, each of the transmittance modes of the LCTF is narrow enough to assume that the radiance information received by the camera when a filter mode is tuned corresponds to the central wavelength alone, i.e., we assume that the modes of the LCTF are equivalent to monochromatic filters. Since the typical spectral accuracy of spectroradiometric devices is 4 nm, monochromatic in this context means to use a spectral width of about that range. The full width at half-maximum (FWHM) of the modes of the LCTF is between 7 and 15 nm,

(a)

(b)

Fig. 4. (a) CIE-31 chromaticity diagram for the 1567 spectral measurements of skylight belonging to the training set. (b) Detail of (a).

(a)

(b)

Fig. 5. (a) CIE-31 chromaticity diagram for the 125 spectral measurements of skylight belonging to the test set. (b) Detail of (a).

depending on the central wavelength chosen, and thus we can accept the assumption of monochromaticity. Second, the radiometric information given by the CCD camera is accurate enough to guarantee that it does not depend on the wavelength, the exposure time, or other external factors. Ferrero et al. [16] described a precise procedure to assure this by means of a complete radiometric calibration eliminating the influence of noise and thus we have followed their recommendations.

The direct radiometric sampling of the visible spectrum consists of tuning the LCTF into a central wavelength between 400 and 720 nm (in 10 nm steps, which are the available modes of our filter) and then taking a picture (corrected for noise influence [16]), of the sky in this case. By doing this, we obtain a radiometric sample of the selected wavelength for every mode of the LCTF, hence covering the whole visible spectrum. This method has the advantage of not needing a training set of spectra, while spectral estimation methods do. Nevertheless, a complete radiometric calibration of the CCD and the filter must be made before using this procedure, and the spectral range covered is reduced to the maximum and minimum central wavelengths achievable with the LCTF. While using the spectral estimation methods, we can obtain information in the whole spectral range covered by the training set, which is usually a little larger, as can be seen in Section 4.

Spectral responsivity $R(\lambda)$ of our monochrome CCD camera was calculated from a proposed model by Ferrero et al. [16]:

$$R(\lambda) = \frac{C^c}{E(\lambda)t_{exp}}, \qquad (7)$$

where C^c refers to the corrected pixel value (eliminating all the possible noise and correcting from spatial nonuniformity [22]), $E(\lambda)$ is the spectral radiance impinging on the CCD, and t_{exp} is the exposure time used for imaging. In this procedure of radiometric sampling, we take one picture for every wavelength selected by the LCTF, which we denote by subindex k. Thus, if we include the effect of filtering at every wavelength by using the LCTF and assume that $E(\lambda)$ remains constant during all the imaging process, we can rewrite Eq. (7) as

$$F_k = \frac{C_k^c}{E_k t_{exp,k}}, \qquad k = 1, \dots\dots 33, \qquad (8)$$

where F_k is equal to the product of the spectral responsivity of the CCD and the LCTF transmittance when mode k is selected and E_k is the value of $E(\lambda)$ at the wavelength chosen by the filter when mode k is tuned. Finally, $t_{exp,k}$ and C_k^c are the exposure time used and the pixel level registered for the corresponding picture, respectively. We can easily calcu-

late the spectral radiance from Eq. (8) as

$$E_k = \frac{C_k^c}{F_k t_{exp,k}}, \qquad k = 1, \dots\dots 33. \qquad (9)$$

In Table 1 we show the mean values (±standard deviations) for the various quality metrics used to compare the similarity between each pair of simultaneous spectra measured with the PR650 and our multispectral system over the set of 125 spectral measurements taken in Granada in 2007 by using the radiometric sampling procedure. Since the test set was acquired with the PR650 spectroradiometer between 380 and 780 nm in steps of 4 nm, and the multispectral system in this radiometric sampling configuration gets spectral information between 400 and 720 nm every 10 nm, a conversion of the data from the PR650 was made prior to comparing the spectra from both instruments. Hence, we discarded the data below 400 nm and above 720 nm, and we made a linear interpolation to get spectral data every 10 nm (some intermediate data were also discarded). The metrics shown [11,23] are the goodness-fit-coefficient (GFC) (which is the cosine of the angle between two spectra if these are intended to be vectors in a Hilbert space), the colorimetric CIELAB ΔE_{ab}^* distance, the percentage of the integrated-radiance-error metric [IRE (%)] (which is a relative measure of the difference in the total energy of the two spectral curves compared), and the colorimetric and spectral combined metric (CSCM) proposed [10,11,23] to compare spectra of natural illuminants from colorimetric and spectral points of view, which has also been used by other researchers [24]. The equations defining these four metrics are shown here ($E(\lambda)$ represents the original spectrum while $E_R(\lambda)$ stands for the recovered spectrum).

$$GFC = \frac{\left| \sum_j E(\lambda_j) E_R(\lambda_j) \right|}{\left| \sum_j [E(\lambda_j)]^2 \right|^{1/2} \left| \sum_j [E_R(\lambda_j)]^2 \right|^{1/2}}, \qquad (10)$$

$$\Delta E_{ab}^* = \sqrt{\Delta L^{*2} + \Delta a^{*2} + \Delta b^{*2}}, \qquad (11)$$

$$IRE(\%) = 100 \frac{\left| \sum_{j=1}^N E(\lambda_j) - E_R(\lambda_j) \right|}{\sum_{j=1}^N E(\lambda_j)}, \qquad (12)$$

Table 1. Mean ± Standard Deviation Values of Various Metrics[a]

GFC	CIELAB ΔE_{ab}^*	IRE (%)	CSCM
0.998 ± 0.002	1.26 ± 0.37	13.10 ± 7.08	15.52 ± 7.33

[a]Over the test set of 125 spectral measurements taken in Granada in 2007 when using the radiometric sampling method

$$\text{CSCM} = \text{Ln}[1 + 1000(1 - \text{GFC})] + \Delta E^*_{ab} + \text{IRE}(\%).\tag{13}$$

We must point out that the CIELAB ΔE^*_{ab} metric is intended to compare two reflectance spectra under a given illuminant and not for comparing illuminants directly. Nevertheless, we can assume that the two SPD of the illuminants we want to compare impinge on a perfectly reflective white patch, and that we are seeing these two assumed patches under the equienergetic (spectrally flat) illuminant. By doing this, we can obtain the CIELAB ΔE^*_{ab} error between two illuminants even though this metric is not intended for this aim.

Three examples of spectral reconstructions made by using this method, corresponding to (a) the 10th, (b) the 50th, and (c) the 90th percentiles of the CSCM metric over the test set of 125 skylight measurements are shown in Fig. 6, where it can be seen how the spectral measurements given by the multispectral system are quite similar to those given by the spectroradiometer PR650, although there is a tendency to overestimate the total energy of the spectra, which implies that high values are obtained for the IRE (%) metric. This could be due to a systematic difference between the theoretically expected pixel values and the real ones, C^c, registered at the camera, which is brought about by the inexact assumption of monochromaticity of the LCTF transmittance modes. Nevertheless, the quality of the spectral measurements taken with the multispectral system in this configuration of radiometric sampling may be accurate enough for certain purposes when studying skylight, where the total energy estimation is not of paramount importance and we may only need the relative SPD.

4. Spectral Estimation Using a Regression Model with 33 Channels

Here we use the information provided by the CCD camera in every one of the 33 available channels of the LCTF to obtain spectral estimations of skylight using both the Imai–Berns and the Linear Pseudoinverse methods referred to in Section 2. The main drawback of using such methods is the need to train the system, i.e., to establish a relationship between the training set of spectra and their known sensors' responses. If we intend to use different test and training sets we cannot also use the set of 125 spectral measurements taken in 2007 as a training set. Thus we should use the set of 1567 skylight spectra measured between 1997 and 1999 as a training set. We must face two drawbacks when using this approach. First, the set of 1567 measurements have a sampling interval of 5 nm, while the test set of 125 measurements have a sampling interval of 4 nm. We solved this problem by making a linear interpolation of the data at 5 nm down to 4 nm, which is not a major source of error since both sampling intervals are accurate enough to register spectral skylight information. The second problem is that we do not have the information re-

lated to the sensors' responses corresponding to those 1567 spectra because our multispectral system was not available at that time. This problem can be solved by simulating the sensors' responses of our system to
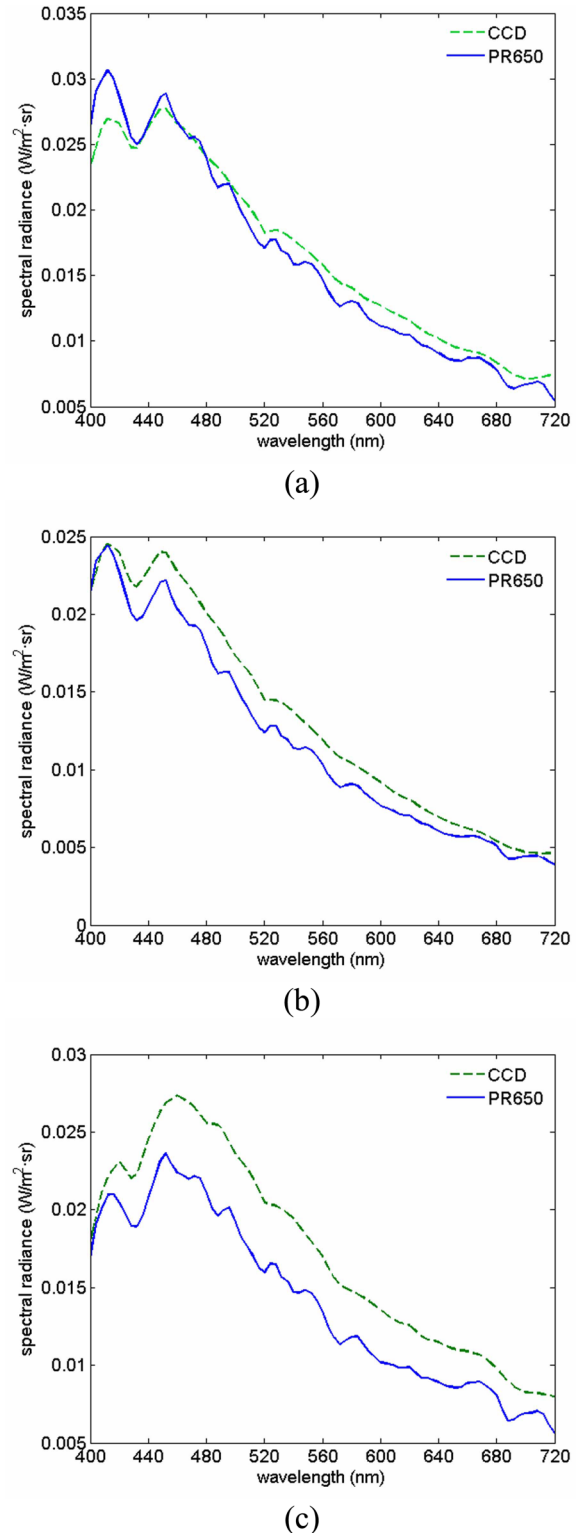

(a)

(b)

(c)

Fig. 6. (Color online) (a) 10th percentile (CSCM = 6.00), (b) 50th percentile (CSCM = 15.35), and (c) 90th percentile (CSCM = 25.05) over the test set of 125 spectral measurements taken in Granada in 2007 when using the radiometric sampling method.

the training set of 1567 spectra [see Eq. (7)], keeping in mind that the spectral responsivity of the camera R is already corrected from noise influence during the calibration [16] (i.e., noise is taken into account in R as explained in Eq. (7) above):

$$C_{k,ts}^c = RE_{ts}t_{exp,k} \qquad (14)$$

and identifying the kth component of the vector ρ of the sensors' responses with the corresponding corrected pixel value divided by the exposure time used for it. Thus,

$$\rho_k = \frac{C_k^c}{t_{exp,k}} \qquad k = 1, \ldots \ldots 33. \qquad (15)$$

If we look at Eq. (5), the spectral estimations are calculated as

$$E_R = X\rho, \qquad (16)$$

where $X = VG$ for the Imai–Berns method and $X = W$ for the Linear Pseudoinverse method [see Eqs. (4) and (6)]. Hence, for the Imai–Berns method we must also select linear basis V of representative vectors, which is unnecessary with the Linear Pseudoinverse method. We choose PCA for constructing this basis because it is the most widely used strategy [1–5,7–11,17,18]. We use different numbers of PCA basis vectors to find the optimum number of them to be used with this multispectral system of 33 channels.

In Table 2 we show the results obtained when we recover the 125 skylight spectra of the test set by using the Linear Pseudoinverse method with the 33 channels available. These results are significantly better than those for the radiometric sampling method in Table 1 (only the GFC metric is slightly worse, probably due to the higher spectral resolution achieved now, as we show below), thus proving that the training of the system by simulating the sensors' responses to the set of 1567 spectra is correct. Figure 7 shows the 10, 50, and 90 percentiles of the CSCM metric when recovering the 125 spectra of the test set with the Linear Pseudoinverse method with 33 channels (just as Fig. 6 did for the radiometric sampling method). Now the spectral range of these estimations is seen to extend to the interval between 380 and 780 nm, which corresponds to the specifications of the spectroradiometer used to measure the training set in 1997 (as mentioned in Section 2), but with a spectral resolution of 4 nm because of the linear interpolation we performed—as we explained above in this

same section—from the original training set sampled at 5 nm. It should also be remembered that the spectral range covered in Section 3 was from 400 nm up to 720 nm, with a spectral resolution of 10 nm, corre-
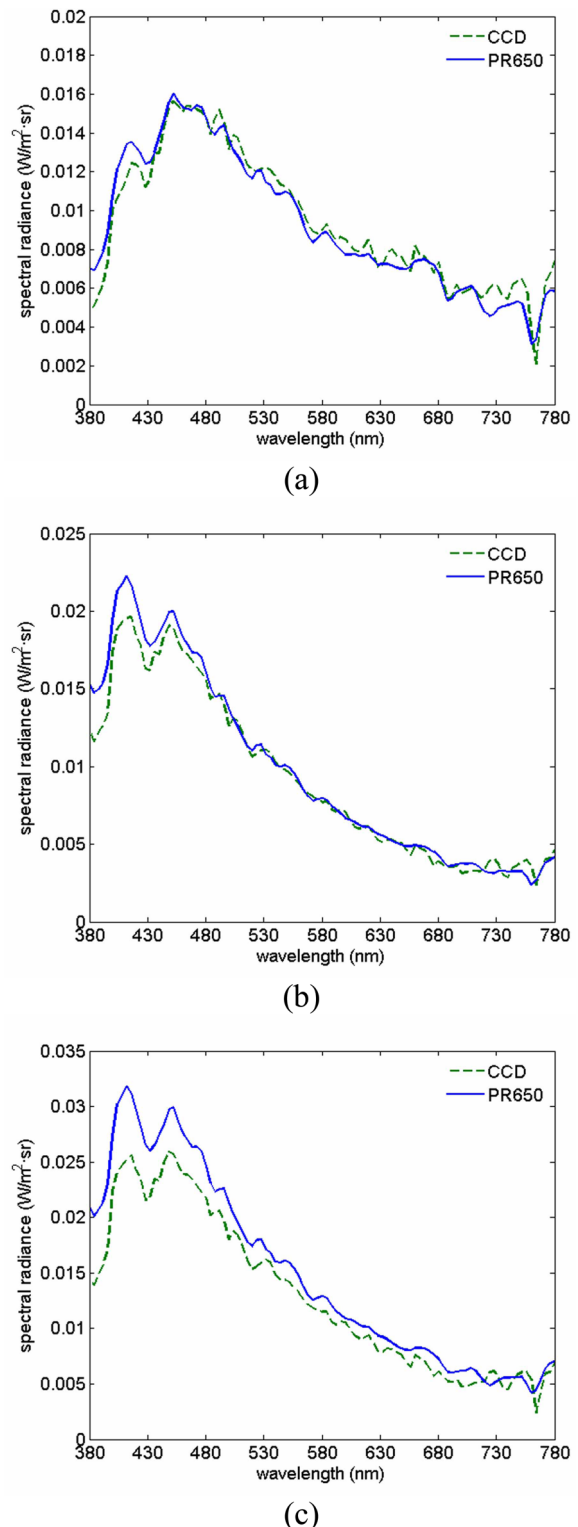

(a)

(b)

(c)

Fig. 7.   (Color online) (a) 10th percentile (CSCM = 3.28), (b) 50th percentile (CSCM = 6.73), and (c) 90th percentile (CSCM = 15.65) over the test set of 125 spectral measurements taken in Granada in 2007 when using the Linear Pseudoinverse method with $k = 33$.

Table 2.   **Mean ± Standard Deviation Values of Various Metrics**[a]

GFC	CIELAB ΔE_{ab}^*	IRE (%)	CSCM
0.998 ± 0.001	0.85 ± 0.21	6.30 ± 5.43	8.51 ± 5.57

[a]Over the test set of 125 spectral measurements taken in Granada in 2007 when using the Linear Pseudoinverse method with 33 channels

sponding to the minimum and maximum central wavelengths tunable with the LCTF (each of these central tunable wavelengths was 10 nm apart from its neighbors). This extension of the spectral range covered will also occur with the Imai–Berns method later; it does not mean that the CCD provides more information now, but that the spectral estimation methods are capable of predicting the spectral shape of the curves throughout the whole range covered by the training set, even if there are no sensors in some spectral regions. This can be done by taking advantage of the statistical information obtained by training the system. Nevertheless, it can be seen in Fig. 7 that the spectral estimations achieved are extremely accurate when compared with the measurements made simultaneously with the PR650, thus proving the Linear Pseudoinverse method's reliability in obtaining good spectral reconstructions of skylight.

In Table 3 we show the results of the Imai–Berns method when using the 33 channels of our system. Different numbers of basis vectors n were used to find the optimum value of this parameter, which turned out to be $n = 6$. Other studies of multispectral systems [2,3,10,11] showed that the best results are found when we use the same number of vectors n as sensors k, but this seems to be true only with a small number of sensors. In Table 3 we have included the case where $n = 101$ because this means that we use all the available PCA vectors, and then the Imai–Berns and the Linear Pseudoinverse methods are formally the same, as can be seen in Eq. (17), which is easily derived from Eqs. (2) and (4)–(6). Thus,

$$E_R = VG\rho = V\varepsilon_{ts}\rho_{ts}^+\rho = E_{ts}\rho_{ts}^+\rho = W\rho, \qquad (17)$$

in which case the results for the Imai–Berns method with $n = 101$ and the Linear Pseudoinverse method are exactly the same (see Tables 2 and 3). The corresponding 10th, 50th, and 90th percentile curves for the Imai–Berns method with $k = 33$ and $n = 6$ are shown in Fig. 8. If we compare Tables 2 and 3 we can see that the Imai–Berns method is slightly better than the Linear Pseudoinverse method when 33 channels are involved because the reduction in dimension-

ality achieved by using $n = 6$ helps to reduce the effect of noise.

5. Spectral Estimation Using Five Optimum Sensors

In Fig. 2 we showed how to implement the five optimum sensors found for the Imai–Berns method (using five PCA vectors) in computational simulations [10] with our LCTF (see Fig. 1) by adjusting the exposure time of each transmittance mode. In this section we show the results obtained when we use our multispectral system in this optimum configuration with only
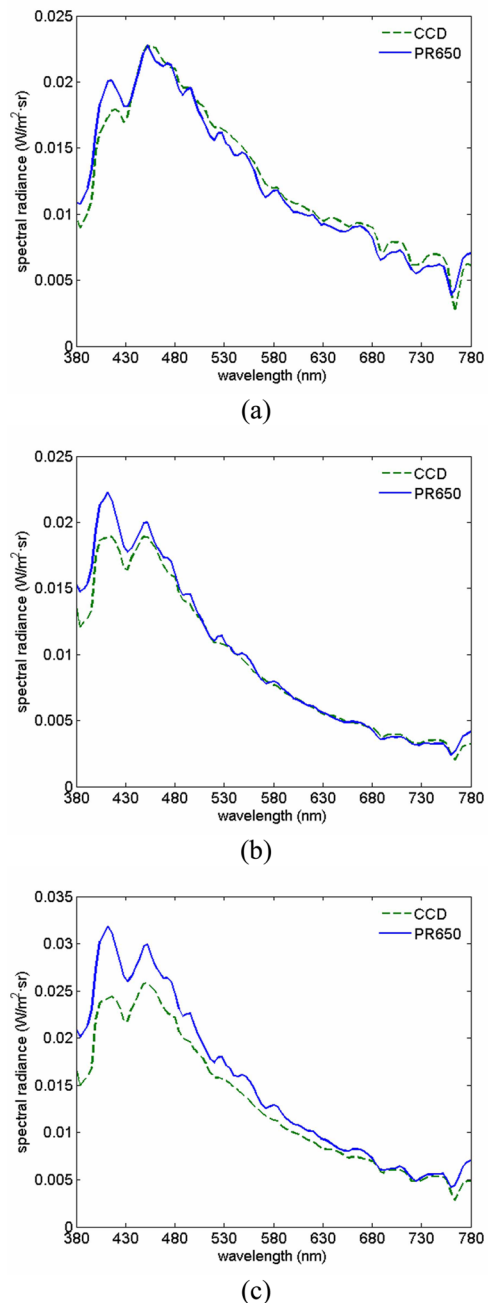

(a)

(b)

(c)

Fig. 8.   (Color online) (a) 10th percentile (CSCM = 3.00), (b) 50th percentile (CSCM = 6.44), and (c) 90th percentile (CSCM = 15.48) over the test set of 125 spectral measurements taken in Granada in 2007 when using the Imai–Berns method with $k = 33$ and $n = 6$.

Table 3.   Mean $\pm$ Standard Deviation Values of Various Metrics[a]

n	GFC	CIELAB ΔE^*_{ab}	IRE (%)	CSCM
3	0.998 ± 0.001	1.19 ± 0.29	6.33 ± 5.28	8.74 ± 5.32
4	0.998 ± 0.001	0.97 ± 0.22	6.33 ± 5.46	8.52 ± 5.58
5	0.998 ± 0.001	0.70 ± 0.23	6.31 ± 5.44	8.24 ± 5.62
6	$\mathbf{0.998 \pm 0.001}$	$\mathbf{0.70 \pm 0.23}$	$\mathbf{6.31 \pm 5.43}$	$\mathbf{8.23 \pm 5.58}$
7	0.998 ± 0.001	0.71 ± 0.23	6.30 ± 5.42	8.26 ± 5.57
8	0.998 ± 0.001	0.88 ± 0.22	6.29 ± 5.41	8.41 ± 5.52
15	0.997 ± 0.001	0.82 ± 0.2	6.31 ± 5.44	8.40 ± 5.59
33	0.997 ± 0.001	0.85 ± 0.21	6.30 ± 5.43	8.49 ± 5.57
101	0.997 ± 0.001	0.85 ± 0.21	6.30 ± 5.43	8.51 ± 5.57

[a]Over the test set of 125 spectral measurements taken in Granada in 2007 when using the Imai–Berns method with 33 channels

seven channels implementing the five intended optimum sensors. We also trained the system here with the 1567 spectra measured in Granada between 1997 and 1999 by simulating their sensors' responses, as shown in Eq. (14). Table 4 shows that the values for the metrics used are very similar to the ones obtained in Section 4 with a larger number of channels. It can also be seen that the spectral curves obtained are very accurate (Fig. 9). The advantage of using this configuration is important, since the spectral estimations are of about the same quality as those in previous sections, but at a fivefold lower cost in time (we use only 7 modes of the LCTF instead of 33, which means a total processing time of 13 s against 1 min). Hence, we strongly recommend an optimization study prior to using the multispectral imaging system.

6. Conclusions

We have proved that accurate multispectral estimations of skylight can be obtained by using a monochrome CCD camera attached to a liquid-crystal tunable filter. The spectral curves of skylight obtained with such a system are very similar to those measured simultaneously with a spectroradiometer but have the several advantages of price, weight, spatial resolution, and portability. Given the spectral similarity of skylight SPDs with any kind of natural illuminant, the multispectral information provided by our multispectral system could be used for many scientific purposes related to the climatology or atmospheric physics.

We tested different configurations of our multispectral system. First, we made use of a complete calibration of the CCD camera and the LCTF to develop a direct radiometric sampling in the visible range of the spectrum. Second, we compared the Linear Pseudoinverse and the Imai–Berns methods when these were used as spectral estimation methods in our multispectral system with 33 channels, and they improved the results obtained with the direct radiometric sampling method. Finally, we implemented the five optimum sensors found in a previous computational study [10] for the Imai–Berns method and showed that they can be implemented by using just seven transmittance modes of the LCTF and adjusting their exposure times. We demonstrated that using a small number of optimum sensors provides almost the same spectral results as using all the available channels of the system, with a significant saving in time. Thus we can recommend developing an optimization procedure prior to building a multispectral system.

Table 4. Mean ± Standard Deviation Values of Various Metrics[a]

GFC	CIELAB ΔE^*_{ab}	IRE (%)	CSCM
0.998 ± 0.001	0.87 ± 0.21	7.05 ± 5.85	8.97 ± 6.00

[a]Over the test set of 125 spectral measurements taken in Granada in 2007 when using the five optimum sensors of the Imai–Berns method with five PCA vectors.
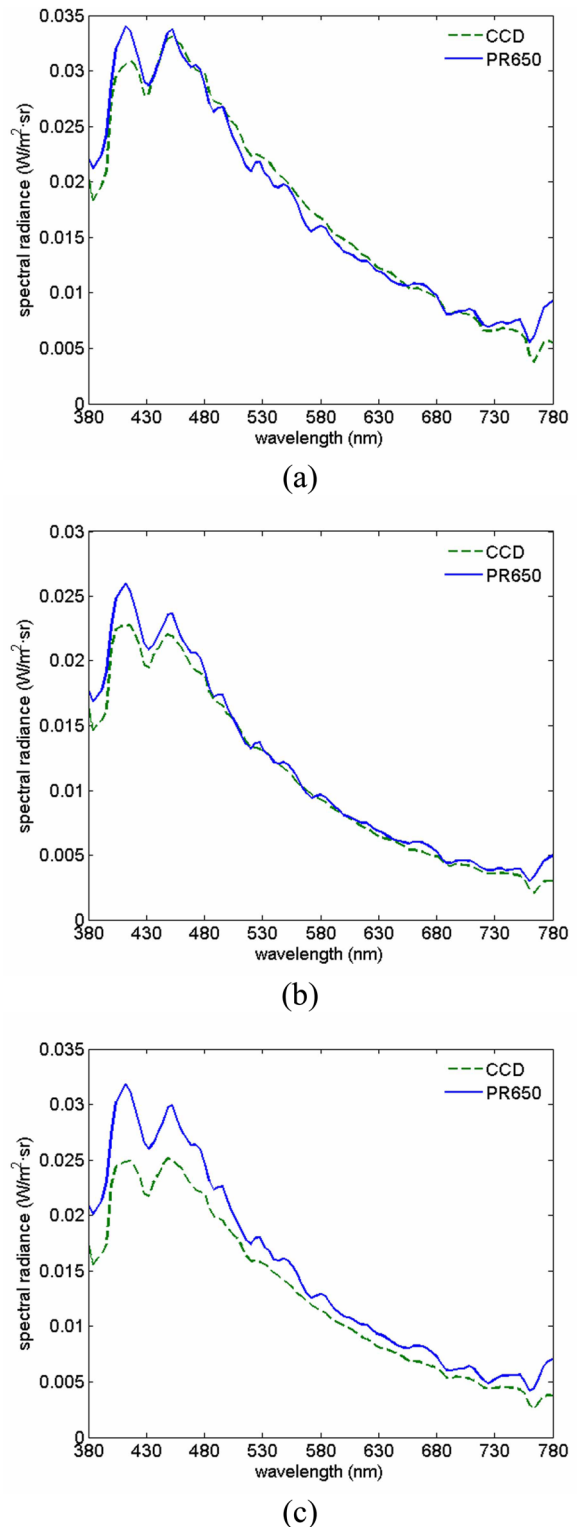

(a)

(b)

(c)

Fig. 9. (Color online) (a) 10th percentile (CSCM = 3.12), (b) 50th percentile (CSCM = 7.48), and (c) 90th percentile (CSCM = 16.76) over the test set of 125 spectral measurements taken in Granada in 2007 when using the Imai–Berns method with five optimum sensors and five PCA vectors.

To conclude, we have demonstrated that the spectroradiometric model proposed theoretically to describe our system does describe its behavior

accurately since the training process using simulated sensors' responses provides spectral reconstructions of high quality when a different test set of 125 spectral curves is recovered.

References

1. J. Y. Hardeberg, "Acquisition and reproduction of color images: colorimetric and multispectral approaches," °Ph.D. dissertation (Ecole Nationale Supérieure des Télécommunications, 1999), pp. 121–174.
2. D. Connah, S. Westland, and M. G. A. Thomson, "Optimization of a multispectral imaging system," in *Proceedings of the 1st European Conference on Colour Graphics, Image and Vision* (Society for Imaging Science and Technology, 2002), pp. 619–622.
3. F. H. Imai and R. S. Berns, "Spectral estimation using trichromatic digital cameras," in *Proceedings of the International Symposium on Multispectral Imaging and Color Reproduction for Digital Archives* (Society of Multispectral Imaging of Japan, 1999), pp. 42–48.
4. H. Haneishi, T. Hasegawa, A. Hosoi, Y. Yokoyama, N. Tsumura, and Y. Miyake, "System design for accurately estimating spectral reflectance of art paintings," Appl. Opt. **39**, 6621–6632 (2000).
5. N. Shimano, "Evaluation of a multispectral image acquisition system aimed at reconstruction of spectral reflectances," Opt. Eng. **44**, 107005 (2005).
6. P. D. Burns and R. S. Berns, "Quantization in multispectral color image acquisition," in *Proceedings of the IS&T 7th Color Imaging Conference: Color Science, Systems and Applications* (Society for Imaging Science and Technology, 1999), pp. 32–35.
7. J. Ho, B. V. Funt, and M. S. Drew, "Separating a color signal into illumination and surface reflectance components: theory and applications," IEEE Trans. Pattern Anal. Mach. Intell. **12**, 966–977 (1990).
8. K. Chandra and G. Healey, "Estimating visible through near-infrared spectral reflectance from a sensor radiance spectrum," J. Opt. Soc. Am. A **21**, 1825–1833 (2004).
9. M. A. López-Álvarez, E. M. Valero, and J. Hernández-Andrés, "Separating illuminant and surface reflectance spectra from filtered trichromatic camera measurements," in *Proceedings of the 3rd European Conference on Colour Graphics, Image and Vision* (Society for Imaging Science and Technology, 2006), pp. 370–373.
10. M. A. López-Álvarez, J. Hernández-Andrés, E. M. Valero, and J. Romero, "Selecting algorithms, sensors and linear bases for optimum spectral recovery of skylight," J. Opt. Soc. Am. A **24**, 942–956 (2007).
11. M. A. López-Álvarez, J. Hernández-Andrés, J. Romero, and R. L. Lee, Jr., "Designing a practical system for spectral imaging of skylight," Appl. Opt. **44**, 5688–5695 (2005).
12. J. L. Nieves, E. M. Valero, S. M. C. Nascimento, J. Hernández-Andrés, and J. Romero, "Multispectral synthesis of daylight using a commercial digital CCD camera," Appl. Opt. **44**, 5696–5703 (2005).
13. R. A. Yotter and D. M. Wilson, "A review of photodetectors for sensing light-emitting reporters in biological systems," IEEE Sens. J. **3**, pp. 288–303 (2003).
14. J. J. Michalsky, "Estimation of continuous solar spectral distributions from discrete filter measurements: II. A demonstration of practicability," Sol. Energy **34**, 439–445 (1985).
15. R. M. Goody and Y. L. Yung, *Atmospheric Radiation, Theoretical Basis*, 2nd ed. (Oxford University Press, 1995), Chap. 5.
16. A. Ferrero, J. Campos, and A. Pons, "Low-uncertainty absolute radiometric calibration of a CCD," Metrologia **43**, S17–S21 (2006).
17. L. T. Maloney and B. A. Wandell, "Color constancy: a method for recovering surface spectral reflectance," J. Opt. Soc. Am. A **3**, 29–33 (1986).
18. M. Shi and G. Healey, "Using reflectance models for color scanner calibration," J. Opt. Soc. Am. A **19**, 645–656 (2002).
19. D. D. Lee and H. S. Seung, "Learning the parts of objects by non-negative matrix factorization," Nature **401**, 788–791 (1999).
20. A. Hyvärinen, J. Karhunen, and E. Oja, *Independent Component Analysis*, 1st ed. (Wiley, 2001), pp. 147–292.
21. J. Hernández-Andrés, J. Romero, and R. L. Lee Jr., "Colorimetric and spectroradiometric characteristics of narrow-field-of-view clear skylight in Granada, Spain," J. Opt. Soc. Am. A **18**, 412–420 (2001).
22. M. de Lasarte, J. Pujol, M. Arjona, and M. Vilaseca, "Optimized algorithm for the spatial nonuniformity correction of an imaging system based on a charged-coupled device color camera," Appl. Opt. **46**, 167–174 (2007).
23. M. A. López-Álvarez, J. Hernández-Andrés, E. M. Valero, and J. L. Nieves, "Colorimetric and spectral combined metric for the optimization of multispectral systems," in *Proceedings of the 10th Congress of the International Colour Association*, J. Hernández-Andrés and J. L. Nieves, eds. (Association Internationale de la Couleur, 2005), pp. 1685–1688.
24. P. A. García, R. Huertas, M. Melgosa, and G. Cui, "Measurement of the relationship between perceived and computed color differences," J. Opt. Soc. Am. A **24**, 1823–1829 (2007).